Journal of the European Ceramic Society **19** (1999) 1027–1031

PII: S0955-2219(98)00366-5
0955-2219/99/$ - see front matter

Hydrothermal Synthesis and Sintering of Electroceramics

Anderson Dias,[a]* Vicente T. L. Buono,[a] Virgínia S. T. Ciminelli[a] and Roberto L. Moreira[b]

[a]Departamento de Engenharia Metalúrgica e de Materiais, EE-UFMG, Rua Espírito Santo 35, 30160-030, Belo Horizonte-MG, Brazil
[b]Departamento de Física, ICEx-UFMG, CP702, 30123-970, Belo Horizonte-MG, Brazil

Abstract

The hydrothermal processing of ultrafine $Pb_{1.88}(Zn_{0.3}Nb_{1.25})O_{5.305}$ *and* $Ba(Mg_{0.33}Nb_{0.67})O_3$ *powders as well as their sintering behavior at 1000°C were investigated. The morphological analyses on nanometric powders indicated the presence of mesopores in micrometric agglomerates with open cylindrical pores. High dielectric constants were observed, showing normal frequency dispersion and an intrinsic* ac *relaxation, relatively masked by low frequency conductivity. The sintered ceramics presented lower dielectric permittivities than the hydrothermal powders, and a classical Cole–Cole plot could be obtained for the* $Pb_{1.88}(Zn_{0.3}Nb_{1.25})O_{5.305}$ *electroceramic for frequencies above* 10^3 *Hz.* © *1999 Elsevier Science Limited. All rights reserved*

Keywords: hydrothermal processing, powders: chemical preparation, sintering, porosity, dielectric properties.

1 Introduction

The studies of barium- and lead-based perovskites have been intensified due to their excellent dielectric and electromechanical properties (large dielectric susceptibility, tunable piezoelectricity, optical birefringence, and nonlinear optical properties). These compounds, often referred to as smart electroceramics,[1,2] are suitable in applications such as multilayer capacitors, transducers, and electro-optic devices.[3,4] The preparation of cubic perovskites is not a trivial task. For example, cubic and rhombohedral pyrochlore phases ($Pb_3Nb_4O_{13}$, $Pb_2Nb_2O_7$ and $Pb_3Nb_2O_8$) are frequently obtained during conventional solid-state reaction to produce $Pb(Zn_{0.33}Nb_{0.67})O_3$.[4,5] The formation of these compounds is detrimental to the dielectric and piezoelectric properties of the perovskite phase, and has also been of concern in many other $A(B_1B_2)O_3$ systems.[6]

There are numerous reports on the preparation of electroceramics by processes such as coprecipitation, sol-gel, and two-step columbite processing.[7,8] The hydrothermal synthesis is sometimes called a 'soft solution chemical processing' because of the mild reaction conditions under which the products are achieved (low temperatures and short reaction times), leading to controlled particle size and morphology.[9–11] These characteristics decrease the sintering temperatures and, consequently, low price products can be obtained.[5,12] In the present work, the hydrothermal synthesis and sintering of $Pb_{1.88}(Zn_{0.3}Nb_{1.25})O_{5.305}$ and $Ba(Mg_{0.33}Nb_{0.67})O_3$, hereafter designated as PZN* and BMN, were investigated. In a previous paper,[13] the hydrothermal process was presented as a new route to produce these electroceramics. Now, the powders morphology and the dielectric properties before and after sintering were analyzed and correlated to the processing conditions.

2 Experimental

Reagent grade lead and zinc nitrates, barium and magnesium chlorides, and niobium oxide were used to synthesize the electroceramics. The salts were dissolved in deionized water (18·2 MΩ.cm) and mixed to the niobium oxide, previously dissolved in hot HF. Sodium hydroxide was vigorously added to the mother solutions until the pH

*To whom correspondence should be addressed. Fax: + 55-31-2381815; e-mail: andias@demet.ufmg.br

value attained 13. The resultant suspensions were transferred to an autoclave equipped with a turbine-type impeller (Parr), and heated at 4°C min^{-1} up to the processing temperature. The syntheses occurred at 200°C for 4 h, under saturated vapor pressure and a stirring speed of 750 rpm. The hydrothermal products were rinsed and dried at 80°C. Green ceramics were prepared by cold pressing the powders at 110 MPa into cylindrical specimens of 3 mm height and 15 mm diameter. Sintering was carried out in air at 1000°C, for 5 h (BMN) and 8 h (PZN*), under heating/cooling rates of 10°C min^{-1}.

X-ray fluorescence (XRF) analyses were conducted using a Philips PW2400 sequential X-ray spectrometer, fitted with an X-ray tube (Rhodium target end window) and Philips SuperQ analytical software. Atomic absorption spectroscopy, energy-dispersive spectrometry (EDS), and scanning electron microscopy (JSM35c and JSM5410) were also employed in the chemical and microstructural characterization of the samples. X-ray powder diffraction (XRD) patterns were recorded in a Philips PW1830 diffractometer, using Cu$K\alpha$ radiation ($\lambda = 0{\cdot}15418$ nm) and a graphite monochromator. The average particle sizes were determined from XRD results (D_{XRD}) by applying the Scherrer equation ($D_{XRD} = 0{\cdot}9\lambda/\beta\cos\theta$),[14] where β is the full-width-at-half-maximum of the main X-ray diffraction peaks. For BMN, the planes used were (102), (202), (104), (204) and (214), while the planes (022), (004), (040) and (305) were employed to calculate D_{XRD} for the PZN* ceramic.

Specific surface areas, hysteresis curves and pore size distributions of the samples were obtained using nitrogen as adsorption/desorption gas (Quantachrome NOVA1000). The powders were vacuum degassed at 200°C for 2 h prior to each analysis. The Brunauer, Emmett and Teller (BET) and the Barrett, Joyner and Halenda (BJH) models were used to determine the surface area and pore size distributions, taken into account the desorption curves.[15] The particle mean size (D_{BET}) was estimated from the values of surface area and density (obtained by helium pycnometry).[15] The agglomerate mean size (D_{50}) of the powders was obtained by Sedigraph and Coulter techniques. Each sample was ultrasonically dispersed (500 W, 5 min) in an aqueous solution containing 0.05 wt% of sodium hexametaphosphate.

Impedance spectroscopy analyses were performed in the frequency range 5–13 MHz, at room temperature, using a computer-controlled Hewlett–Packard Model 4192A equipment. Disk-like samples (typical dimensions: 200–250 mm^2 of area and 2–3 mm of thickness) were gold plated before electrical measurements.

3 Results and Discussion

The hydrothermal conditions employed in the present work led to a homogeneous precipitation of the ceramic powders, according to the following global reactions:

$$1{\cdot}88Pb(NO_3)_2 + 0{\cdot}3Zn(NO_3)_2{\cdot}6H_2O + 0{\cdot}625Nb_2O_5 + 4{\cdot}36NaOH \Rightarrow Pb_{1{\cdot}88}(Zn_{0{\cdot}3}Nb_{1{\cdot}25})O_{5{\cdot}305} + 4{\cdot}36NaNO_3 + 3{\cdot}98H_2O \text{ and} \quad (1)$$

$$3BaCl_2{\cdot}2H_2O + MgCl_2{\cdot}6H_2O + Nb_2O_5 + 8NaOH \Rightarrow 3Ba(Mg_{1/3}Nb_{2/3})O_3 + 8NaCl + 16H_2O. \quad (2)$$

Single-phase BMN perovskite powders were obtained after hydrothermal processing, with only some impurities related to sodium salts and niobium unknown phases.[13] Single-phase and impurity free BMN ceramic bodies were also obtained after 5 h of heating treatment at 1000°C. PZN* was the main product from the hydrothermal treatment at 200°C and also after sintering.[13] The elemental analyses of the hydrothermal ceramics, as determined by atomic absorption spectroscopy, EDS, and XRF showed that iron was the main impurity in PZN* and BMN powders. XRF spectrum also presents manganese and strontium as contaminants in BMN, which were not detected by EDS. No traces of other elements were found on PZN* samples by the above-mentioned techniques.

Submicrometer-sized particles arranged in agglomerates were observed in both hydrothermal powders; Fig. 1 shows the green microstructure for the PZN* electroceramic. According to Roosen and Hausner,[16] the fabrication of high-technology materials with reproducible properties demands an

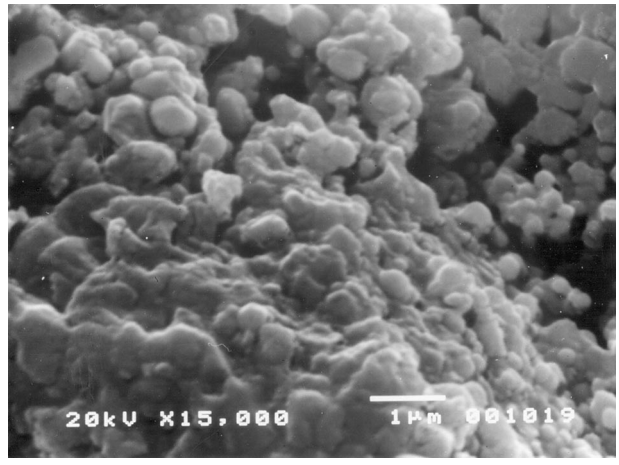

Fig. 1. SEM micrograph of the hydrothermal PZN* powder.

improved processing of submicrometer powders, since it is well know that nanocrystalline particles tend to agglomeration. However, these authors show that the hydrothermal treatment leads to a very narrow particle size distribution with few and loosed agglomerates. During compaction, the agglomerates are easily destroyed enabling the formation of homogeneous pore structures in the green compact (this result holds for our materials, as it is observed in Fig. 1). The sintered PZN* (Fig. 2) is formed by uniform grains of about 1 μm in diameter, with some bigger grains related to the pyrochlore phase. EDS analyses performed on the sintered samples indicated that there is no variation in the elemental composition at micrometer level.

The nitrogen adsorption/desorption curves (hysteresis curves) for the hydrothermal powders are presented in Fig. 3, which shows that the ceramics contain cylindrical mesopores open at both ends.[15] First, the presence of mesopores is observed through the adsorption isotherm: the slope increases at higher relative pressures and the inflection point represents the completion of the first adsorbed monolayer. Second, the approximately cylindrical geometry is expected when pores of a given radius fill at higher relative pressures than when empty. Figure 3 also shows that the volume of nitrogen adsorbed by PZN* powders was higher than that adsorbed by BMN ceramics. A thin hysteresis was observed for this material, indicating its higher homogeneity in terms of porosity. The pore size distributions, obtained from desorption curves, corroborate this result (inset in Fig. 3). Most frequent pores of around 10 nm in BMN and 7 nm in PZN* were found and probably dominate the pore structure of these materials. The weight of the nitrogen adsorbed monolayer on the surface of the hydrothermal powders was around 8 mg for BMN and 22 mg for PZN*, showing that the later is more porous than the BMN powder (note that both materials were produced at identical conditions of temperature and time).

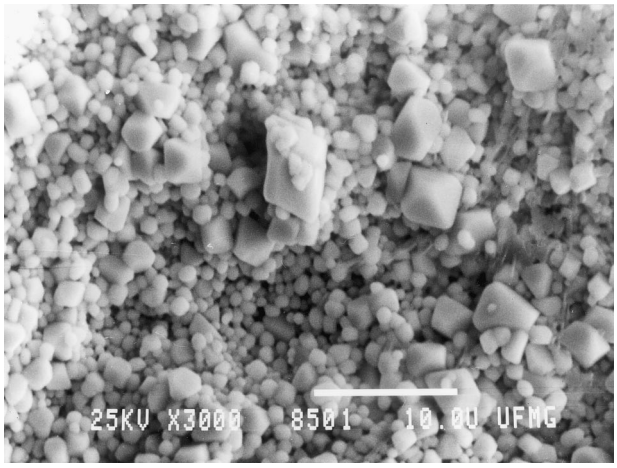

Fig. 2. SEM fractured surface for the sintered PZN* ceramic.

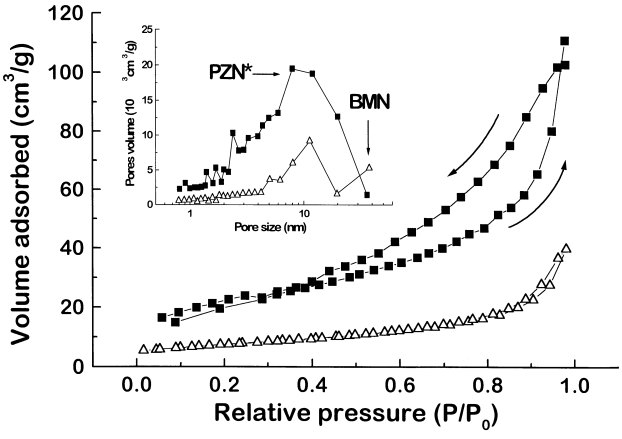

Fig. 3. Adsorption/desorption isotherms for the hydrothermal powders. Inset: pore size distributions.

Table 1 presents the main morphological parameters of the materials studied here: total volume of pore (V_T), pores mean size (D_p), specific surface area (S), and true density (ρ). From these results, the particle sizes (D_{BET}) of the samples could be calculated[15] and were found to be in the nanometric range (Table 1). Together with submicrometer-sized particles, the agglomeration state of the powders acts in the sintering process increasing or decreasing the reactivity of the material, thus influencing the sintering kinetics.[12] In this work, the agglomerate mean size (D_{50}) was inferred through Sedigraph and Coulter techniques. The last columns of the Table 1 shows D_{50} obtained from Sedigraph (D_{50S}) and Coulter (D_{50C}) for PZN* and BMN ceramics. This morphological parameter provides an indication, for a given material and dispersing condition, of the agglomeration state of the samples. A higher value of D_{50} was observed for BMN, which presents lower specific surface area and higher particle size than PZN*.

The processes of densification and grain growth, which occur during sintering, are directly related to particle size, powder morphology, agglomeration state and impurity level.[17] It was verified that the surface chemistry of nanoparticles governs the surface and grain-boundary diffusion, the dominant

Table 1. Morphological parameters of the hydrothermal electroceramics

Sample	V_T ($10^3 cm^3 g^{-1}$)	D_p (nm)	S ($m^2 g^{-1}$)	ρ ($g cm^{-3}$)	D_{BET} (nm)	D_{XRD} (nm)	D_{50S} (μm)	D_{50C} (μm)
PZN*	171·3	4·6	75·2 ± 0·6	5·78	14	12 ± 1	1·2	3·4
BMN	61·6	4·7	26·5 ± 0·4	4·91	46	36 ± 13	1·8	4·1

processes during sintering.[12,17] Also, powder agglomeration is strongly influenced by the surface chemistry. In the present work, we believe that the hydrothermal treatment of hydroxide suspension obtained after chemical preparation leads to elimination of the hydroxyl groups. Consequently, for a given material, smaller agglomerates are observed for powders with lower porosity levels.

Let us now discuss the dielectric properties of the electroceramics hydrothermally produced. It was observed in ceramic powders as well as in the sintered bodies high dielectric constants with a decreasing tendency for increasing frequencies. Also, a relaxation could be observed for both materials in spite of the higher low frequency conductivity, which tends to mask the relaxation. For PZN*, this relaxation can be clearly seen for the hydrothermal powder as well as for the sintered body, although a deviation of the Debye behavior was observed at low frequencies (see Fig. 4). The complex relative dielectric constant is given by:[18,19]

$$\varepsilon^* = \varepsilon' - j[\varepsilon'' + (\sigma^*/\omega\varepsilon_0)] \tag{3}$$

where ε' is the relative dielectric constant, ε'' the relative excess (*ac*) dielectric loss, and $\sigma^*/\omega\varepsilon_0$ the charge carriers contribution to the dielectric response (σ^* is the complex low frequency conductivity, $j = \sqrt{-1}$, and ε_0 the permittivity of free space). In order to get quantitative information from the experimental data, a variety of different theoretical models developed to describe dielectric relaxation phenomena were applied. For our results, the best fit between theoretical and experimental curves was found with the classical Cole–Cole model (exemplified by the full line in Fig. 4). In this model, the real and imaginary parts (ε' and ε'') of the dielectric constant are written as:[18,19]

$$\varepsilon' - \varepsilon_\infty = \{(\varepsilon_s - \varepsilon_\infty)|1 + (\omega\tau_0)^{1-\alpha}\sin(\alpha\pi/2)|\}/ \{1 + 2(\omega\tau_0)^{1-\alpha}\sin(\alpha\pi/2) + (\omega\tau_0)^{2(1-\alpha)}\} \text{ and} \tag{4}$$

$$\varepsilon'' = \{(\varepsilon_s - \varepsilon_\infty)(\omega\tau_0)^{1-\alpha}\cos(\alpha\pi/2)\}/ \{1 + 2(\omega\tau_0)^{1-\alpha}\sin(\alpha\pi/2) + (\omega\tau_0)^{2(1-\alpha)}\}, \tag{5}$$

where ε_∞ is the instantaneous permittivity, ε_s is the static permittivity, τ_0 is the time constant and α is a distribution parameter for the relaxation times ($0 \le \alpha \le 1$; for Debye relaxation, $\alpha = 0$). The term $(\varepsilon_s - \varepsilon_\infty)$ is referred sometimes as the relaxation strength, $\Delta\varepsilon$.

The sintered PZN* material presented lower dielectric permittivities than the hydrothermal powder and a classical Cole–Cole plot[18] could be obtained for frequencies above 10^3 Hz, as showed in Fig. 4. The center of the arc is submerged below the real axis, indicating a relatively sharp distribution of relaxation times. The deviation of the data in the low frequency side of this figure is due to the important contribution of charge carrier conductivity to the dielectric response [the last term of eqn (3), which is not taken into account in eqns (4) and (5)]. By using impedance spectroscopy, one may distinguish between processes running at different rates, e.g. between the transport across the grain boundary and the transport within the grain (bulk). Consequently, one can determine average local quantities, e.g. the grain boundary resistance and thickness, the bulk conductivity and the dielectric constant. The modeling according Cole–Cole[18] of our results, full-line in Fig. 4, provided the following parameters: $\varepsilon'_s = 208$ (bulk and grain boundary resistance), $\varepsilon'_\infty = 8$ (bulk resistance) and $\alpha = 0.11$ (sharp distribution of relaxation times). The dielectric constant relaxation time (τ) is the relaxation time obtained from the frequency at which the excess (*ac*) dielectric loss attains its maximum, $\omega\tau = 1$, or the frequency of the inflection point in the dispersion of the relative dielectric constant versus frequency. For the sintered PZN* studied here, the relaxation time was $\tau_0 = 12$ kHz.

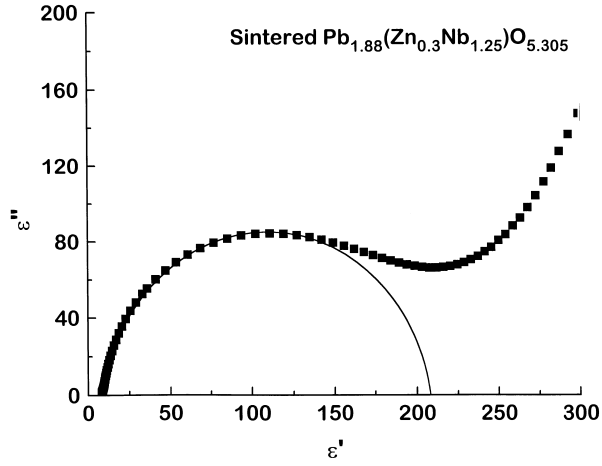

Fig. 4. Argand diagram for the PZN* ceramic sintered at 1000°C for 8 h. The full-line represents the modeling according to Cole–Cole.[18]

The observed relaxation can be intimately related to the relaxor nature of the material. The high relaxation strength ($\Delta\varepsilon = 200$), the low instantaneous permittivity ($\varepsilon_\infty = 8$), and the 12 kHz relaxation time at room temperature indicate that the (relaxor) technological applications of our PZN* ceramic are optimized below 10 kHz. Concerning the sintered BMN, although a small relaxation around 10^2 Hz could be observed, the high *dc* conductivity masks the intrinsic *ac* relaxation and a treatment using eqns (4) and (5) gives poorest results. Additional investigations should be done to

determine the nature (extrinsic or intrinsic) of the low frequency conductivity and to reveal the intrinsic ac relaxation.

In summary, the hydrothermal process was used to produce single-phase PZN* and BMN electroceramics. Morphological analyses showed nanometric powders with high surface areas, which enhanced the sintering kinetics. High permittivities were observed for the sintered ceramics and a dielectric relaxation was clearly verified for the PZN* sample.

Acknowledgements

This work was partially supported by the Brazilian agencies CNPq and FAPEMIG.

References

1. Materials for smart systems. *Mater. Res. Soc. Symp. Proc. 360, Boston (1994)*, eds. E. P. George, S. Takahashi, S. T. McKinstry, K. Uchino and M. W. Fogle. MRS, Pittsburgh, Pennsylvania, 1995.
2. Newnham, R. E. and Ruschau, G. R., *J. Am. Ceram. Soc.*, 1991, **74**, 463.
3. Akbas, M. A. and Davies, P. K., *J. Mater. Res.*, 1997, **12**, 2617.
4. Yoon, K. H., Kim, S. Y. and Kang, D. H., *J. Mater. Res.*, 1995, **10**, 939.
5. Shrout, T. R. and Halliyal, A., *Am. Ceram. Soc. Bull.*, 1987, **66**, 704.
6. Lu, C., *J. Mater. Sci.*, 1996, **31**, 699.
7. Halliyal, A., Kumar, U., Newnham, R. E. and Cross, L. E., *Am. Ceram. Soc. Bull.*, 1987, **66**, 671.
8. Fijiu, T., Tanaka, A. and Takenaka, T., *Jpn. J. Appl. Phys.*, 1991, **30**, L298.
9. Dias, A. and Buono, V. T. L., *J. Mater. Res.*, 1997, **12**, 3278.
10. Dias, A., Buono, V. T. L., Vilela, J. M. C., Andrade, M. S. and Lima, T. M., *J. Mater. Sci.*, 1997, **32**, 4715.
11. Dias, A., Moreira, R. L., Mohallem, N. D. S., Vilela, J. M. C. and Andrade, M. S., *J. Mater. Res.*, 1998, **13**, 223.
12. Dias, A., Mohallem, N. D. S. and Moreira, R. L., *Mater. Res. Bull.*, 1998, **33**, 475.
13. Dias, A., Buono, V. T. L., Ciminelli, V. S. T. and Moreira, R. L., *J. Korean Phys. Soc.*, 1998, **32**, 1187.
14. *International Union of Crystallography. International Tables for X-ray Crystallography*, Part III, Dorbrecht, The Netherlands, 1985, pp. 318–323.
15. Lowell, S. and Shields, J. E., *Powder Surface Area and Porosity*, Chapmann & Hall Ltd., New York, 1987.
16. Roosen, A. and Hausner, H., *Adv. Ceram. Mater.*, 1988, **3**, 131.
17. Ready, M. J., Lee, R. R., Halloran, J. W. and Heuer, A. H., *J. Am. Ceram. Soc.*, 1990, **73**, 1499.
18. Cole, R. H. and Cole, K. S., *J. Chem. Phys.*, 1941, **9**, 341.
19. Jonscher, A. K., *IEEE Trans. on Electr. Insul.*, 1992, **27**, 407.